

# A comparative study between vision transformers and CNNs in digital pathology

Luca Deiningger<sup>1</sup>

deiningger.luca@gmail.com

Bernhard Stimpel<sup>1</sup>

bernhard.stimpel@roche.com

Anil Yuce<sup>1</sup>

anil.yuce@roche.com

Samaneh Abbasi-Sureshjani<sup>1</sup>

samaneh.abbasi@roche.com

Simon Schönenberger<sup>1</sup>

simon.schoenenberger@gmail.com

Paolo Ocampo<sup>2</sup>

ocampo.paolo-santiago@gene.com

Konstanty Korski<sup>1</sup>

konstanty.korski@roche.com

Fabien Gaire<sup>1</sup>

fabien.gaire@roche.com

<sup>1</sup> F. Hoffmann-La Roche AG, Grenzacherstrasse 124, 4070 Basel, Switzerland

<sup>2</sup> Genentech, Inc., 1 DNA Way, South San Francisco, CA 94080, USA

## Abstract

Recently, vision transformers were shown to be capable of outperforming convolutional neural networks when pretrained on sufficient amounts of data. In comparison to convolutional neural networks, vision transformers have a weaker inductive bias and therefore allow a more flexible feature detection. Due to their promising feature detection, this work explores vision transformers for tumor detection in digital pathology whole slide images in four tissue types, and for tissue type identification. We compared the patch-wise classification performance of the vision transformer *DeiT-Tiny* to the state-of-the-art convolutional neural network *ResNet18*. Due to the sparse availability of annotated whole slide images, we further compared both models pretrained on large amounts of unlabeled whole-slide images using state-of-the-art self-supervised approaches. The results show that the vision transformer performed slightly better than the *ResNet18* for three of four tissue types for tumor detection while the *ResNet18* performed slightly better for the remaining tasks. The aggregated predictions of both models on slide level were correlated, indicating that the models captured similar imaging features. All together, the vision transformer models performed on par with the *ResNet18* while requiring more effort to train. In order to surpass the performance of convolutional neural networks, vision transformers might require more challenging tasks to benefit from their weak inductive bias.

## 1. Introduction

Convolutional neural networks (CNNs) are a powerful tool for tumor detection in digital pathology whole-slide images (WSIs) reaching accuracies of over 90% for patch-wise tumor detection depending on the type of cancer [15, 25, 26, 29]. CNNs have been the common architecture for digital pathology tasks, but the more recently in-

roduced vision transformers (ViTs) [7] have not been fully investigated in this domain yet. In comparison to CNNs, ViTs are free of convolution-induced biases which allows the model to learn global features and complex relations in the data. Dosovitskiy *et al.* [7] showed that their entirely convolution-free ViT can outperform CNNs such as *ResNet* [12]. Also considering the strength of transformers for natural language processing [6, 17, 20, 31], this raises the question whether ViTs are the next big model in image recognition and whether those will replace CNNs in the future.

Despite the triumph of ViTs, their weak inductive bias is also a limiting factor. Meaning, those models require large amounts of training data to surpass the performance of CNNs [7, 27]. Touvron *et al.* [27] aimed for training ViTs on datasets of the same size as comparable CNNs. They introduced the data-efficient vision transformer tiny (*DeiT-Tiny*), which we focus on in this work. Beyond architectural model adjustments, transfer learning can overcome the difficulty of training vision transformers as it improves model convergence for downstream tasks [21]. In digital pathology, models pretrained on ImageNet [5] are common. However, more recent work showed the potential of models pretrained on digital pathology datasets [1]. Especially self-supervised pretraining is interesting in this domain due to the sparse availability of annotated WSIs. This allows the model to learn features on large amounts of data, which might boost the performance for downstream tasks on unseen datasets. A recent promising self-supervised approach for ViT training is DINO [4]. The authors of DINO present their method as self-distillation with no labels and showed that the extracted self-supervised DINO features are powerful for other downstream image classification tasks. Even though their method is not restricted to ViTs, the authors demonstrate that the DINO architecture works especially well for those models.

Due to their emerging potential, this work explores fully- and self-supervised (DINO) ViTs for patch-wise tu-

mor detection in sentinel lymph node (SLN), diffuse large B-cell lymphoma (DLBCL), breast, and lung adenocarcinoma (LUAD) WSIs. Furthermore, we benchmarked the models on tissue type identification in colorectal cancer WSIs. To evaluate the potential of ViTs, we compared their performance to the state-of-the-art CNN *ResNet18* and analyzed the qualitative differences in their classifications.

## 2. Materials and Methods

This section presents the configuration of the fully- and self-supervised ViT and the setup of the baseline *ResNet18*. Moreover, it explains the datasets used for the two downstream tasks tumor detection and tissue type identification.

### 2.1. Fully-supervised models

#### 2.1.1 Model configuration

In this work, we used the *ResNet18* pretrained on ImageNet as the baseline classifier, as it provides a good trade-off between classification accuracy and training time for the tasks considered in this work. For the ViT, we used the data-efficient image transformer tiny (*DeiT-Tiny*) with patch size 16, pretrained on ImageNet [27].

For both models, we changed the number of neurons in the last fully-connected layer to the number of target classes.

#### 2.1.2 Model training

The fully-supervised models used the *Cross-entropy Loss* weighted according to inverse class frequencies and trained for up to 300 epochs using batch size 128. The *ResNet18* based models used *Adam* [16] with  $\beta_1 = 0.9$ ,  $\beta_2 = 0.98$ , learning rate  $1e^{-6}$ , and L2 regularization ( $1e^{-3}$ ). The *DeiT-Tiny* used *sharpness-aware minimization* (SAM) [8] using the implementation from Samuel [22] with stochastic gradient descent (SGD), learning rate  $1e^{-3}$  and momentum 0.9. The idea of SAM is to simultaneously minimize the loss value and the loss sharpness. It seeks model parameters that lie in neighborhoods having a low loss. For this purpose, SAM performs two forward-backward passes for gradient descent which results in a longer training time in comparison to Adam. Initially, we used Adam for ViT optimization but we observed that the model did not achieve the same classification performance as the *ResNet18*. SAM greatly improved ViT generalization in comparison to Adam at the cost of an increased runtime.

To speed up the training time per epoch, the models used balanced sampling of the training patches and stratified subsampling of the validation patches, resulting in roughly 100,000 training and 50,000 validation patches per epoch.

In order to prevent overfitting, the models used an *augmentations* (version 0.5.2) [3] image augmentation pipeline

comprising *ColorJitter*, vertical and horizontal flip, and 90 degree rotation. Furthermore, the models used early stopping with 30 epochs patience to prevent overfitting.

### 2.2. Self-supervised models

For self-supervised ViT pretraining, we utilized DINO [4] with a *DeiT-Tiny* backbone and trained it on what we call the TCGA 100 dataset. We refer to this model as *DINO* in the following. The TCGA 100 dataset comprises patches from 8,747 *The Cancer Genome Atlas* (TCGA) WSIs encompassing the datasets BRCA, CHOL, HNSC, KIRC, KIRP, LIHC and PRAD. These slides come from around 20 different tissue types. The models randomly sampled 100,000 training and 50,000 validation patches at each epoch to reduce the training time per epoch, and trained for 100 epochs. Furthermore, the models used  $256 \times 256$  images instead of  $224 \times 224$  images as in the original DINO implementation.

For transfer to tumor detection and tissue type identification, we used the *DINO* teacher as a *DeiT-Tiny* backbone and trained it in a fully-supervised manner as explained in Sec. 2.1.2. In addition to this setup, we trained the neural network classifier only and fixed the weights in the feature extraction layers to speed up downstream training. We refer to this setting as FW ('fixed weights') in the following sections. For tissue type identification, we further used image up-scaling to  $256 \times 256$  to fit the pretrained *DINO* backbone architecture.

As a self-supervised CNN, we used the *ResNet18* pretrained in a self-supervised manner on a digital pathology dataset, termed as *PathNet* [1]. *PathNet* was trained with *Bootstrap Your Own Latent* (BYOL) [10] on eight tissue types: DLBCL, lymph node, follicular lymphoma, tonsil, lung, colon, breast and thyroid. The reader is referred to Abbasi-Sureshjani *et al.* [1] for details on model pretraining. For transfer to downstream tasks, we trained it as described in Sec. 2.1.2.

### 2.3. Performance evaluation

In order to assess the model performance for tumor detection, we calculated the area under the precision-recall curve (PR AUC). For tissue type identification, we macro averaged the PR AUC for each class (one vs. rest) to retrieve one value. Since accuracy is the most frequently reported metric in the literature, we also report it for the comparison of our models to state-of-the-art approaches.

### 2.4. Model comparison

In order to assess the similarity of *ResNet18* and *DeiT-Tiny* predictions, we calculated the Pearson correlation [9] of the mean patch-wise accuracy of the test slides. Moreover, we computed a two-sided p-value which indicates the probability of uncorrelated model predictions

that have a Pearson correlation at least as extreme as the one computed [28]. For attention heatmap creation, we used *Gradient-weighted Class Activation Mapping (Grad-CAM)* [23]. Our implementation used the last feature extraction layer as the model target layer and backpropagated the label of the model’s own prediction.

## 2.5. Datasets

### 2.5.1 Tissue type identification

For tissue type identification we used the CRC9 dataset [13] comprising 100,000 non-overlapping  $224 \times 224$  color-normalized [18] patches at magnification  $20\times$  (0.5 microns per pixel [MPP]). The patches originate from hematoxylin & eosin (H&E) stained histological images of human colorectal cancer (CRC) and normal tissue, and are categorized in nine classes. Our models used 70% of the data for training, 15% for validation and 15% for testing.

### 2.5.2 Tumor detection

For all tumor detection tasks, we used our internal tissue segmentation software to determine the WSI tissue region. Patches belonging to the tumor class were obtained through exhaustive (all tumor lesions in a slide were annotated) and non-exhaustive pathologist tumor annotations. The patches belonging to the non-tumor (normal) class were obtained either from WSIs of tissues known to contain no tumor lesions, or from regions outside the pathologist exhaustive tumor lesion annotations. If not otherwise mentioned, we extracted  $256 \times 256$  patches at magnification  $20\times$  (0.5 MPP) with an overlap of at least 90% with the desired region (tumor or normal) and sampled 75% of the slides for training and 25% for validation while using an independent test set.

We benchmarked our models on four tissue types. We used the Camelyon16 dataset [2] for SLN metastatic tumor detection which comprises 270 training and 130 test WSIs from two independent medical centers. For DLBCL tumor detection, we trained and tested on 4,957 and 103 internal WSIs, respectively. Those WSIs comprised non-tumoral tonsil and lymph node tissue, and lymph node tissue with DLBCL tumor. For breast tumor detection, we trained and tested on 335 and 537 internal breast WSIs, respectively. For LUAD tumor detection, we trained and tested on 431 and 138 internal lung WSIs, respectively. For details, see Supplementary.

## 3. Results

In this section, we present the results for patch-wise tissue type identification, and tumor detection for several tissue types. We compared the performance of the CNNs *ResNet18* and *PathNet* to the ViTs *DeiT-Tiny* and *DINO*. Furthermore, we compared their classifications on slide level.

## 3.1. Performance comparison across all datasets

The comparison of the test PR AUC values across all datasets, shown in Tab. 1, demonstrates that the performance of the *ResNet18*, *PathNet*, the *DeiT-Tiny* and *DINO* were very similar. For DLBCL, the *ResNet18* performed slightly better while the ViT-based models performed slightly better for SLN, LUAD and breast.

Table 1. Model test PR AUC and accuracy (ACC). For datasets with multiple test sets (LUAD and breast), we show the un-weighted mean per dataset.

Model	FW	Metric	CRC9	SLN	DLBCL	LUAD	Breast
<i>ResNet18</i>	×	PR AUC	<b>0.999</b>	0.885	<b>0.976</b>	0.913	0.809
		ACC	<b>0.995</b>	0.981	<b>0.88</b>	0.858	0.915
<i>DeiT-Tiny</i>	×	PR AUC	0.998	<b>0.917</b>	0.97	<b>0.94</b>	0.817
		ACC	0.982	<b>0.988</b>	0.874	0.88	0.913
<i>PathNet</i>	×	PR AUC	<b>0.999</b>	0.908	0.97	0.92	0.818
		ACC	<b>0.995</b>	0.979	0.866	<b>0.885</b>	0.92
<i>DINO</i>	×	PR AUC	<b>0.999</b>	0.912	0.958	0.933	<b>0.828</b>
		ACC	0.991	0.984	0.874	0.871	<b>0.924</b>

During early experiments with SLN tumor detection, we assessed whether the *DeiT-Tiny* benefits from more WSI context. Thus, we trained and tested the models on  $10\times$  magnification. The performance was very similar to training on  $20\times$ . On  $10\times$ , the *ResNet18* and the *DeiT-Tiny* reached a test PR AUC of 0.887 and 0.919, respectively.

To place our results in context to existing work, we compared our results to state-of-the-art methods on the same digital pathology tasks. All together, our results are on par with the state-of-the-art performances on the same digital pathology tasks [11, 14, 19, 24, 30, 32]. However, the results are not directly comparable due to differences in the datasets and test splits used.

### 3.2. PathNet vs. DINO

We observed that when fixing the weights in the feature extraction layers and using the extracted features directly, *PathNet* performed better than *DINO* for DLBCL only (Tab. 2). For CRC9, SLN, LUAD and breast, *DINO* performed better which we hypothesize is explained by the different dataset that it was trained on. TCGA 100 contains more diverse tissue types thus the network has learned a better phenotype representation. This suggests to consider *DINO* for embedding extraction for downstream tasks, since it is more versatile than *PathNet*.

Table 2. Comparison of *PathNet* and *DINO* test PR AUC and accuracy for fixing weights in model feature extraction layers.

Model	FW	Metric	CRC9	SLN	DLBCL	LUAD	Breast
<i>PathNet</i>	✓	PR AUC	0.969	0.833	<b>0.931</b>	0.887	0.711
		ACC	0.928	0.943	<b>0.829</b>	0.859	0.883
<i>DINO</i>	✓	PR AUC	<b>0.997</b>	<b>0.894</b>	0.887	<b>0.914</b>	<b>0.751</b>
		ACC	<b>0.983</b>	<b>0.959</b>	0.817	<b>0.878</b>	<b>0.897</b>

### 3.3. Model comparison

In order to compare the *ResNet18* and *DeiT-Tiny* predictions, we calculated the mean patch-wise accuracy of the test slides for every dataset. The comparison shows a correlation of the mean test slide accuracies for SLN, DLBCL and breast with exception of a few outliers (Fig. 1). For LUAD, we hypothesize that mainly smaller slides cause the larger accuracy fluctuations.

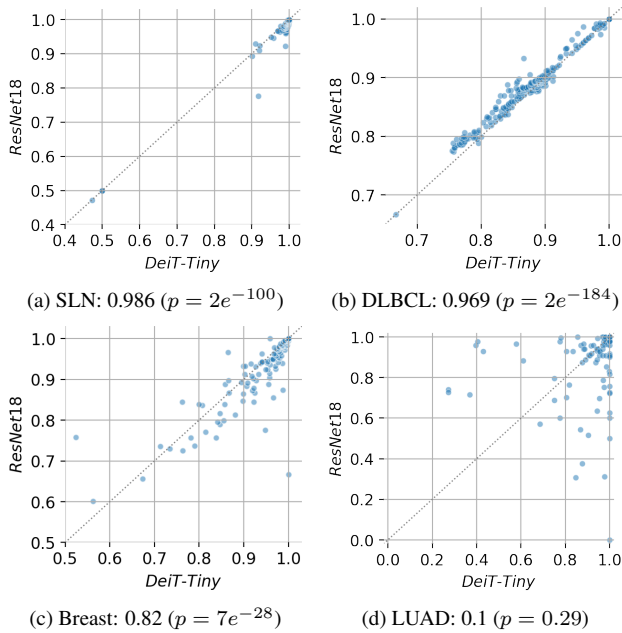


Figure 1. Mean accuracy per test slide incl. Pearson correlation.

A comparison of *ResNet18* and *DeiT-Tiny Grad-CAM* heatmaps shows that the ViT focused on more localized patch regions in comparison to the CNN (Fig. 2). While the benefit is not evident for tumor detection, this might be important for other tasks in digital pathology.

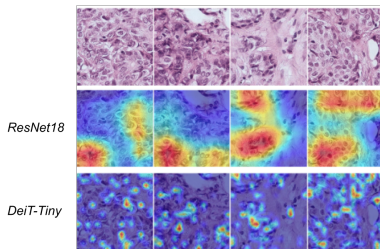


Figure 2. Comparison of *ResNet18* and *DeiT-Tiny Grad-CAM* heatmaps for randomly selected SLN tumor patches. Both models classified all shown patches correctly with a probability of  $> 0.9$ .

### 3.4. Runtime comparison

As Tab. 3 shows, the *DeiT-Tiny* throughput is twice as slow as the *ResNet18* throughput due to SAM which needs to perform two forward-backward passes for training.

Table 3. Throughput comparison of *ResNet18* and *DeiT-Tiny* for full training pipeline.

Model	#params	Throughput (img/s)
<i>ResNet18</i>	11M	250
<i>DeiT-Tiny</i> (Adam)	5M	238
<i>DeiT-Tiny</i> (SAM)	5M	117

## 4. Conclusion

ViTs show emerging potential in the field of image classification due to their weak inductive bias in comparison to CNNs which allows them to understand complex relationships in the data. To assess whether this also holds for tasks in digital pathology, this work explored fully- and self-supervised ViTs for tissue type identification and tumor detection in WSIs.

The benchmark on several datasets showed that the ViT-based models performed similar to the baseline *ResNet18* across several datasets and across different magnifications. Latter observation suggests that neither the *ResNet18* nor the *DeiT-Tiny* showed a benefit from more WSI context. The comparison of the classifications on slide level showed that the predictions of the *ResNet18* and ViT-based models are correlated. This indicates that both the *ResNet18* and the ViT captured similar image features. Interestingly, we observed that *DINO* is more versatile than *PathNet* for tumor detection across several tissue types and thus offers an interesting alternative to the *PathNet* backbone. However, the higher performance of *DINO* is most likely caused by a more diverse dataset trained on.

Considering the similar performances across several datasets and magnifications, the correlation of slide-wise accuracies and the costly ViT training, the *DeiT-Tiny* performed on par with the *ResNet18* while requiring more training effort. We hypothesize that digital pathology tissue type identification and tumor detection are tasks that can be easily learned with traditional CNN approaches. Consequently, ViTs often could not benefit from its larger flexibility in feature detection in comparison to the CNNs. Therefore, we propose the application of ViTs to more challenging digital pathology tasks that for example require more contextual knowledge.

### Acknowledgements

The authors would like to thank Roche Diagnostic Solutions, Roche Life Cycle and the Roche Study team for providing the data, as well as the Roche Personalized Healthcare Digital Pathology Program for funding this work. Some of the results presented here are based upon data generated by the TCGA Research Network: <https://www.cancer.gov/tcga>. The authors declare the following competing interests: A.Y., B.S., S.A., F.G. and K.K. are employees of Roche, L.D. and S.S. were employed by Roche at the time of this work and P.O. is employee of Genentech.



## References

- [1] Samaneh Abbasi-Sureshjani, Anil Yüce, Simon Schönberger, Maris Skujevskis, Uwe Schalles, Fabien Gaire, and Konstanty Korski. Molecular subtype prediction for breast cancer using H&E specialized backbone. In *Proceedings of the MICCAI Workshop on Computational Pathology*, volume 156 of *Proceedings of Machine Learning Research*, pages 1–9. PMLR, 27 Sep 2021. 1, 2
- [2] Babak Bejnordi, Mitko Veta, Paul Johannes van Diest, Bram van Ginneken, Nico Karssemeijer, Geert Litjens, Jeroen A. W. M. van der Laak, , and the CAMELYON16 Consortium. Diagnostic Assessment of Deep Learning Algorithms for Detection of Lymph Node Metastases in Women With Breast Cancer. *JAMA*, 318(22):2199–2210, 12 2017. 3
- [3] A. Buslaev, A. Parinov, E. Khvedchenya, V. I. Iglovikov, and A. A. Kalinin. Albumentations: fast and flexible image augmentations. *ArXiv e-prints*, 2018. 2
- [4] Mathilde Caron, Hugo Touvron, Ishan Misra, Hervé Jégou, Julien Mairal, Piotr Bojanowski, and Armand Joulin. Emerging properties in self-supervised vision transformers, 2021. 1, 2
- [5] Jia Deng, Wei Dong, Richard Socher, Li-Jia Li, Kai Li, and Li Fei-Fei. Imagenet: A large-scale hierarchical image database. In *2009 IEEE conference on computer vision and pattern recognition*, pages 248–255. Ieee, 2009. 1
- [6] Jacob Devlin, Ming-Wei Chang, Kenton Lee, and Kristina Toutanova. BERT: Pre-training of deep bidirectional transformers for language understanding, 2018. 1
- [7] Alexey Dosovitskiy, Lucas Beyer, Alexander Kolesnikov, Dirk Weissenborn, Xiaohua Zhai, Thomas Unterthiner, Mostafa Dehghani, Matthias Minderer, Georg Heigold, Sylvain Gelly, Jakob Uszkoreit, and Neil Houlsby. An image is worth 16x16 words: Transformers for image recognition at scale, 2020. 1
- [8] Pierre Foret, Ariel Kleiner, Hossein Mobahi, and Behnam Neyshabur. Sharpness-aware minimization for efficiently improving generalization. *CoRR*, abs/2010.01412, 2020. 2
- [9] David Freedman, Robert Pisani, and Roger Purves. Statistics (international student edition). *Pisani, R. Purves, 4th edn. WW Norton & Company, New York*, 2007. 2
- [10] Jean-Bastien Grill, Florian Strub, Florent Altché, Corentin Tallec, Pierre H. Richemond, Elena Buchatskaya, Carl Doersch, Bernardo Avila Pires, Zhaohan Daniel Guo, Mohammad Gheshlaghi Azar, Bilal Piot, Koray Kavukcuoglu, Rémi Munos, and Michal Valko. Bootstrap your own latent: A new approach to self-supervised learning, 2020. 2
- [11] Bijaya Kumar Hatuwal and Himal Chand Thapa. Lung cancer detection using convolutional neural network on histopathological images. *International Journal of Computer Trends & Technology*, 68(10):21–24, Oct. 2020. 3
- [12] Kaiming He, Xiangyu Zhang, Shaoqing Ren, and Jian Sun. Deep residual learning for image recognition, 2015. 1
- [13] Jakob Nikolas Kather, Niels Halama, and Alexander Marx. 100,000 histological images of human colorectal cancer and healthy tissue, Apr. 2018. 3
- [14] Jakob Nikolas Kather, Johannes Krisam, Pornpimol Charoentong, Tom Luedde, Esther Herpel, Cleo-Aron Weis, Timo Gaiser, Alexander Marx, Nektarios A. Valous, Dyke Ferber, Lina Jansen, Constantino Carlos Reyes-Aldasoro, Inka Zörnig, Dirk Jäger, Hermann Brenner, Jenny Chang-Claude, Michael Hoffmeister, and Niels Halama. Predicting survival from colorectal cancer histology slides using deep learning: A retrospective multicenter study. *PLOS Medicine*, 16(1):e1002730, Jan. 2019. 3
- [15] Sana Ullah Khan, Naveed Islam, Zahoor Jan, Ikram Ud Din, and Joel J. P. C Rodrigues. A novel deep learning based framework for the detection and classification of breast cancer using transfer learning. *Pattern Recognition Letters*, 125:1 – 6, 2019. 1
- [16] Diederik P. Kingma and Jimmy Ba. Adam: A method for stochastic optimization, 2017. 2
- [17] Yinhan Liu, Myle Ott, Naman Goyal, Jingfei Du, Mandar Joshi, Danqi Chen, Omer Levy, Mike Lewis, Luke Zettlemoyer, and Veselin Stoyanov. RoBERTa: A robustly optimized BERT pretraining approach, 2019. 1
- [18] Marc Macenko, Marc Niethammer, J. S. Marron, David Borland, John T. Woosley, Xiaojun Guan, Charles Schmitt, and Nancy E. Thomas. A method for normalizing histology slides for quantitative analysis. In *2009 IEEE International Symposium on Biomedical Imaging: From Nano to Macro*. IEEE, June 2009. 3
- [19] Weiming Mi, Junjie Li, Yucheng Guo, Xinyu Ren, Zhiyong Liang, Tao Zhang, and Hao Zou. Deep learning-based multi-class classification of breast digital pathology images. *Cancer Management and Research*, Volume 13:4605–4617, June 2021. 3
- [20] Alec Radford, Jeff Wu, Rewon Child, David Luan, Dario Amodei, and Ilya Sutskever. Language models are unsupervised multitask learners. 2019. 1
- [21] Hariharan Ravishankar, Prasad Sudhakar, Rahul Venkataramani, Sheshadri Thiruvankadam, Pavan Annangi, Narayanan Babu, and Vivek Vaidya. Understanding the mechanisms of deep transfer learning for medical images, 2017. 1
- [22] David Samuel. PyTorch implementation of SAM optimizer. <https://github.com/davda54/sam>, 2020. 2
- [23] Ramprasaath R. Selvaraju, Michael Cogswell, Abhishek Das, Ramakrishna Vedantam, Devi Parikh, and Dhruv Batra. Grad-CAM: Visual explanations from deep networks via gradient-based localization. 2016. 3
- [24] Georg Steinbuss, Mark Kriegsmann, Christiane Zgorzelski, Alexander Brobeil, Benjamin Goeppert, Sascha Dietrich, Gunhild Mechttersheimer, and Katharina Kriegsmann. Deep learning for the classification of non-hodgkin lymphoma on histopathological images. *Cancers*, 13(10):2419, May 2021. 3
- [25] Sairam Tabibu, P. K. Vinod, and C. V. Jawahar. Pan-renal cell carcinoma classification and survival prediction from histopathology images using deep learning. *Scientific Reports*, 9(1), July 2019. 1
- [26] Muhammed Talo. Automated classification of histopathology images using transfer learning. *Artificial Intelligence in Medicine*, 101:101743, 11 2019. 1
- [27] Hugo Touvron, Matthieu Cord, Matthijs Douze, Francisco Massa, Alexandre Sablayrolles, and Hervé Jégou. Training

data-efficient image transformers & distillation through attention, 2020. 1, 2

- [28] Pauli Virtanen, Ralf Gommers, Travis E. Oliphant, Matt Haberland, Tyler Reddy, David Cournapeau, Evgeni Burovski, Pearu Peterson, Warren Weckesser, Jonathan Bright, Stéfan J. van der Walt, Matthew Brett, Joshua Wilson, K. Jarrod Millman, Nikolay Mayorov, Andrew R. J. Nelson, Eric Jones, Robert Kern, Eric Larson, C J Carey, İlhan Polat, Yu Feng, Eric W. Moore, Jake VanderPlas, Denis Laxalde, Josef Perktold, Robert Cimrman, Ian Henriksen, E. A. Quintero, Charles R. Harris, Anne M. Archibald, Antônio H. Ribeiro, Fabian Pedregosa, Paul van Mulbregt, and SciPy 1.0 Contributors. SciPy 1.0: Fundamental Algorithms for Scientific Computing in Python. *Nature Methods*, 17:261–272, 2020. 3
- [29] Duc My Vo, Ngoc-Quang Nguyen, and Sang-Woong Lee. Classification of breast cancer histology images using incremental boosting convolution networks. *Information Sciences*, 482:123 – 138, 2019. 1
- [30] Shidan Wang, Tao Wang, Lin Yang, Donghan M. Yang, Junya Fujimoto, Faliu Yi, Xin Luo, Yikun Yang, Bo Yao, ShinYi Lin, Cesar Moran, Neda Kalhor, Annikka Weissferdt, John Minna, Yang Xie, Ignacio I. Wistuba, Yousheng Mao, and Guanghua Xiao. Conypath: A software tool for lung adenocarcinoma digital pathological image analysis aided by a convolutional neural network. *EBioMedicine*, 50:103–110, 2019. 3
- [31] Zhilin Yang, Zihang Dai, Yiming Yang, Jaime Carbonell, Ruslan Salakhutdinov, and Quoc V. Le. XLNet: Generalized autoregressive pretraining for language understanding, 2019. 1
- [32] Chuang Zhu, Fangzhou Song, Ying Wang, Huihui Dong, Yao Guo, and Jun Liu. Breast cancer histopathology image classification through assembling multiple compact CNNs. *BMC Medical Informatics and Decision Making*, 19(1), Oct. 2019. 3

# Supplementary - *A comparative study between vision transformers and CNNs in digital pathology*

## 1. Dataset details

The following tables show an overview of the datasets used for colorectal cancer (CRC) tissue type identification (Tab. 1), sentinel lymph node (SLN, Tab. 2), diffuse large B-cell lymphoma (DLBCL, Tab. 3), breast (Tab. 4) and lung adenocarcinoma (LUAD, Tab. 5).

Table 1. CRC9 dataset: number of patches for training and testing.  
Number of patches for training include patches for validation.

Class	Training	Test
TUM	12,169	2,148
MUS	11,506	2,030
LYM	9,823	1,734
DEB	9,785	1,727
BACK	8,981	1,585
STR	8,879	1,567
ADI	8,846	1,561
MUC	7,562	1,334
NORM	7,449	1,314

Table 2. SLN: number of extracted patches.

Magnification	Class	Training	Test
20×	Normal	2,520,477	1,312,918
	Tumor	60,719	52,506
10×	Normal	638,555	333,719
	Tumor	15,035	13,081

Table 3. DLBCL datasets. DLBCL train and test are internal datasets.

Dataset	# slides	# normal patches	# tumor patches
Camelyon16 Train	248	2,520,477	-
Camelyon16 Test	128	1,312,918	-
DLBCL train	4,581	30,333,616	13,923,512
DLBCL test	103	145,693	479,818
Total	5,060	34,312,704	13,923,512

Table 4. Breast cancer datasets. Non TCGA datasets are internal datasets.

Dataset	# slides	# normal patches	# tumor patches
TCGA train	167	84,471	616,963
Breast train	168	30,423	154,243
TCGA test 2	64	37,270	222,789
Breast test 2	45	13,681	37,037
Breast test 1	333	25,138	675,864
TCGA test 1	95	67,139	369,991
Total	872	258,122	2,076,887

Table 5. LUAD datasets.

Dataset	# slides	# normal patches	# tumor patches
Lung train	382	104,750	255,455
TCGA_LUAD train	49	45,905	176,650
Lung test 1	94	45,748	91,107
Lung test 2	44	31,160	40,063
Total	569	227,563	563,275